

## Research Article

# Experimental Investigation on Microstructure and Mechanical Properties of Friction Welded Dissimilar Alloys

**Arun Negemiya Arulsamy** <sup>1</sup>, **Gnanasekaran S,** **Bakkiyaraj Murugesan** <sup>2</sup>,  
**Samson Jerold Samuel Chelladurai** <sup>3</sup>, **Mohanraj Kishnan Selvaraj,**<sup>1</sup>  
**Vijayakumar Palanivel,**<sup>1</sup> and **Gizachew Balcha** <sup>4</sup>

<sup>1</sup>Department of Mechanical Engineering, Sri Shakthi Institute of Engineering and Technology, Coimbatore 641062, Tamil Nadu, India

<sup>2</sup>Department of Mechanical Engineering, Rajalakshmi Institute of Technology, Chennai 600124, Tamil Nadu, India

<sup>3</sup>Department of Mechanical Engineering, Sri Krishna College of Engineering and Technology, Coimbatore, Tamil Nadu, India

<sup>4</sup>Department of Chemical Engineering, College of Biological and Chemical Engineering, Addis Ababa Science and Technology University, Addis Ababa, Ethiopia

Correspondence should be addressed to Gizachew Balcha; [gizachew.balcha@aastu.edu.et](mailto:gizachew.balcha@aastu.edu.et)

Received 8 January 2022; Revised 10 November 2022; Accepted 16 November 2022; Published 9 December 2022

Academic Editor: Ismael Alejandro Aguayo-Villarreal

Copyright © 2022 Arun Negemiya Arulsamy et al. This is an open access article distributed under the Creative Commons Attribution License, which permits unrestricted use, distribution, and reproduction in any medium, provided the original work is properly cited.

High-temperature dissimilar connections built of Inconel 718 and AISI 410 martensitic stainless steel (MSS) are widely used in a range of industries, including boiler construction, the chemical industry, aerospace, and nuclear. When compared to other materials, Inconel 718 and AISI 410 martensitic stainless steel offer superior strength and corrosion resistance under a variety of environmental conditions. The rotational speed was adjusted between 1100 and 1500 RPM, while the friction pressure, friction time, forging pressure, and forging duration were all kept constant during the testing. Five sets of testing were performed, with the resultant tensile strength (both room temperature and hot tensile) and Vickers Hardness being recorded for each set of trials. To assess the structural integrity of the joints, a detailed microstructural investigation, SEM-EDS, and XRD were performed at their interfaces. Mechanical properties were revealed to be high at 1300 RPM due to the small grain size at the interface region; ultimate tensile strength and hardness were determined to be 571 MPa and 423 HV, respectively, due to the small grain size at the interface region. Additionally, a pitting corrosion study has been conducted on dissimilar welded joints at optimum conditions, and their results were discussed and compared with base metals.

## 1. Introduction

Dissimilar metals are frequently more difficult to combine than similar metals because of the variations in physical, chemical, and metallurgical qualities of the parent metals. There are a variety of extremely efficient solid-state joining methods being explored for the joining of incompatible materials, including explosion welding, diffusion welding, and cold roll welding. Rotary friction welding (RFW) is a solid-state welding method that is extensively used in the automotive, aeronautical, and railway industries. It is possible to connect two parts using this technique by clamping

one, while the other rotates and is forged onto the weld surface [1–4]. Once a sufficient amount of frictional heat has been produced, the spindle breaks, and the two pieces are forced together. The most important bonding processes are diffusion and, in the case of two different materials, the development of intermetallic phases. Diffusion is the most important bonding mechanism. As a result of the lack of a need for filler wire throughout the operation, the weld quality is superior to that of traditional fusion welding methods. Other important considerations are the symmetry of the joint, the stability of the process, the shortest possible cycle durations, and the narrow heat-affected zone of the

joint. Due to the elevated local temperature and internal pressure [5–9], the joint has a limited heat-affected zone and the material has been distorted plastically. The rotating speed, friction pressure, friction time, forging pressure, and forging time are the most important factors to consider while doing continuous drive rotary friction welding.

At present, rotary friction welding is used to join different materials such as copper, aluminum, titanium, and steel with one another. Alloy 718 is a NiFe-based superalloy that has been reinforced with Ni<sub>3</sub>Nb and shows exceptional corrosion resistance, as well as remarkable mechanical characteristics when exposed to high temperatures. Fusion welding methods such as electron beam welding, tungsten inert gas welding, and laser welding [10–14] are frequently used to join alloy 718 together. Alloy 718 has certain flaws connected to it, such as the development of the leaves phase, microfissuring, and Niobium segregation, which are all caused by the fusion welding process. It is possible that this will occur in the fusion zone or heat-affected zone (HAZ) and will impair the strength and service life [15–17]. The use of a solid-state welding technique such as friction welding may provide an alternate connecting approach that will solve these problems. The mechanical characteristics of AISI 410 martensitic stainless steel and the nickel-based superalloy Inconel 718 are excellent, as is their corrosion resistance [18–22]. High temperature and corrosive environments are common in the power plant and chemical industries, and the dissimilar combination is frequently used in the production of turbine blades, air intake fans, combustion chamber exhaust systems, control systems, and compressor blades in jet engines, among other applications. The main components of the next-generation boiler (ultracritical boiler), including the superheater and turbine, are constructed of AISI410 and Inconel 718 dissimilar joint fabrication. It is less expensive in terms of cost than nickel alloy when using martensitic stainless steel. The dissimilar junction of Inconel 718 and AISI 410 significantly lowers material costs while providing excellent operating performance in high-temperature and corrosive environments, among other benefits. From the past research literature, we concluded that no researcher had done substantial studies on the FW of dissimilar joints between the Inconel 718 and AISI410 materials regarding metallurgical and corrosion studies. Hence, the present investigation aims to fill that gap.

## 2. Experimental Details

**2.1. Material Selection.** Rotary friction welded connections were constructed from Inconel 718 and AISI 410 martensitic stainless steel with a diameter of 12 mm and a length of 75 mm for a cylindrical rod with a diameter of 12 mm and a length of 75 mm. Using an abrasive cutting machine, the workpiece was cut, and uneven surfaces were eliminated by lathe facing and disc polishing (800–2000 grit emery sheets) before being polished using a disc polisher. The chemical composition of the basic material is shown in Table 1 of this document. The mechanical characteristics of basic materials are given in Table 2. The optical micrographs of the base materials are exposed in Figure 1. It can be observed that the

TABLE 1: Chemical composition of Inconel 718 and AISI410 (wt %).

Material	Ni	Cr	Mo	Nb	Ti	Mn	C	Al	Fe
AISI 410	0.75	13.5	–	–	–	1	0.15	–	Bal
Inconel718	Bal	19	3	4.97	0.9	0.8	0.04	0.5	18.5

microstructure (Figure 1(a)) of Inconel 718 has a coaxial grain structure in the  $\gamma$  matrix and that there are only minor quantities of annealing twins present [23–26]. The presence of annealing twins is only possible in the FCC crystal structure. Fine carbide depressed in a soft ferrite matrix is evident in the MSS (Figure 1(b)), and a ferrite structure with fine carbide depressed in a soft ferrite matrix is also visible [27, 28].

### 2.2. Friction Welding Setup and Testing Procedure.

Fabrication of the joints was accomplished using continuous drive friction welding equipment. Figure 2 depicts the initial configuration of the workpiece setup arrangement (make: RV machine tools, Model: SPM-10). The three-jaw chuck was used to build this machine in two different configurations. To apply friction pressure and forging pressure, one jaw was moveable in an anticlockwise direction, while the other jaw was fixed but could be moved forward and backward in any direction. Inconel 718 was installed in the rotating three-jaw chuck, whereas AISI 410 was installed in the stationary three-jaw chuck. The welding machine's control unit was programmed with the necessary parameters (Table 3) that were fixed (rotational speed, friction pressure, friction time, forging pressure, and forging time). To achieve the desired rotational speed, both workpieces must be exposed to rubbing action under the influence of the axial force. Because of the rubbing action, heat was produced between the workpiece and metals that reached temperatures below the melting point. In addition, an axial shortening was induced under the axial force, which allowed the metals to be connected.

### 2.3. Testing and Characterization Methods.

This experiment changed one parameter while keeping the other values constant. To achieve ideal joints, many weld experiments were carried out, and for each parameter, five joints were made: tensile test sample, notch tensile test sample, hardness sample preparation, and microstructure sample preparation. Figure 3 depicts the tensile test sample produced by the ASTM E8M standard, while Table 4 lists the findings. The rotational speed varied between 1100 and 1500 rpm, while the friction pressure, friction time, forging pressure, and forging time remained constant. Using Vickers microhardness testing equipment under optimal welding circumstances, the hardness of dissimilar joints is determined. When a load of 500 g was applied and the dwell duration was 15 sec, the hardness of the joints was measured along the welded zone of the joints made from Inconel 718 base metal to AISI 410 base metal in a different location along the welded zone. Optical microscopy (OM) was used to investigate the microstructure of improved welded connections. A variety of grain-size emery sheets (500, 1000, 1500,

TABLE 2: Mechanical properties of Inconel 718 and AISI410.

Sl.No.	Base metal	Yield strength (MPa)	Ultimate tensile strength (MPa)	Elongation (%)	Hardness (HV)
1	Inconel 718	1100	1375	20	220
2	AISI 410	415	713	25	188



FIGURE 1: Base metal microstructure (a) Inconel 718 and (b) AISI 410.

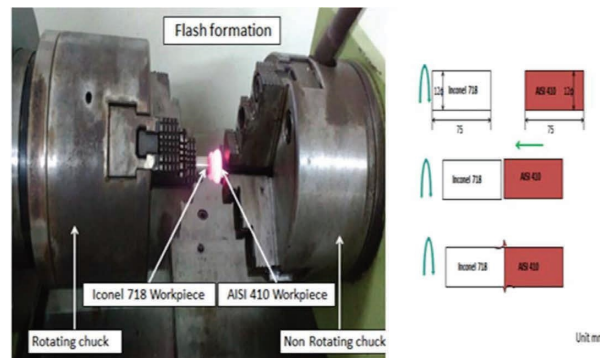


FIGURE 2: The machine setup for welding.

TABLE 3: Welding parameters.

Sample no.	Speed (rpm)	Friction Pressure (MPa)	Friction Time (sec)	Forging Pressure (MPa)	Forging Time (sec)
1.	1100	188.95	10	188.95	10
2.	1200	188.95	10	188.95	10
3.	1300	188.95	10	188.95	10
4.	1400	188.95	10	188.95	10
5.	1500	188.95	10	188.95	10

2000, and 2500) and diamond polishing were used to mechanically polish the specimens before they were polished with diamonds.

#### 2.4. Pitting Corrosion Behavior for Optimized Condition.

The joint fabricated at 1300 rpm rotation speed was taken into account for corrosion studies as the joint exhibits maximum strength at the same speed and the joint results were compared with the base metals. To carry out the potentiodynamic polarization examination, the welded joint and base metal specimens were prepared with a 20 mm × 20 mm square shape and a 5 mm thickness. A

software-integrated Gill AC Potentiostat system was used in this study with a working medium of 3.5% NaCl solution. A scan rate of 0.5 mV/sec was adopted to plot the polarization measurement as polished specimens were kept in the solution for one hour in an immersed state. The polarization examination was conducted two times on each sample to ensure repeatability.

### 3. Results and Discussion

**3.1. Mechanical Properties Characterization.** In this study, it was discovered that the tensile strength rises as the rotational speed increases from 1100 rpm to 1300 rpm and that the



FIGURE 3: Tensile test specimen dimension, before test, and after test specimens.

TABLE 4: Mechanical properties of Inconel 718 and AISI 410 dissimilar joints.

Sample no.	Speed (rpm)	Failure region	Yield strength (MPa)	Ultimate tensile strength (MPa)	Elongation (%)
1.	1100	Interface	460	497	22
2.	1200	Interface	465	500	24
3.	1300	Interface	533	571	27
4.	1400	Interface	524	560	24
5.	1500	Interface	498	532	25

tensile strength progressively declines beyond that point. The tensile strength was determined to be 497 MPa at the lowest rotational speed of 1100 rpm and progressively rose to 571 MPa at the highest rotational speed of 1300 rpm. The insufficient amount of heat produced at low rotational speed (1100 rpm) for a consistent friction pressure and friction duration results in poorer welding because there is not enough heat generated to soften the metal to form a connection. The metals to be connected are exposed to high heat and subsequent cooling at a quicker rate when they are rotated at a high rotational speed. Consequently, metals become more malleable, allowing them to soften more readily, resulting in a decreased tensile strength after 1300 rpm. At 1300 rpm, a sufficient quantity of heat is produced, resulting in increased tensile strength of the material. At the speed of 1500 rpm, more plasticized materials were expelled from the interface of the joint as a result of the generation of friction heat that was higher than the sufficient limit. This is attributed to reduced joint strength. It is consistent with the previous researcher [29, 30]. The change in tensile strength as a function of rotating speed is shown in Table 4.

**3.2. Macrostructure Characterization.** Following the findings of this research, it was discovered that the macrostructures of Inconel 718 and AISI 410 dissimilar joints

exhibit a considerable variance in the flash generation due to the varied heat input, as shown in Figure 4, and are significantly different from one another. Based on the macrostructure, it is evident that flash production is minimal at 1100 rotational speed, and it has also been noticed that the flash radius increases as the rotational speed increases. The increase in flash radius may be caused by the heat produced at the contact during rotary friction welding operations. It is also apparent from the macrostructural research that the width of the heat-affected area increases up to the rotational speed of 1300 rpm, and that the width of the heat-affected region decreases later on, even though the rotational speed is raised. A possible explanation for this change in the heat-affected breadth is the increased rate at which surplus heat is dissipated into the environment. For this reason, as the rotational speed increases, the rate of localized melting (deformation) accelerates, and the fully deformed metal at the interface moves out within a fraction of a second, resulting in a high amount of heat being generated at the interface that dissipates into the surrounding atmosphere rather than affecting the metals to be joined.

According to the findings of the macrostructural investigation, the flash generation rate was higher in martensitic stainless steel (AISI 410) than in nickel-based superalloy (SU 718). Due to the increased hardness of the nickel-based superalloy, there may be an excess of flash generation (SU 718). This property of the nickel-based



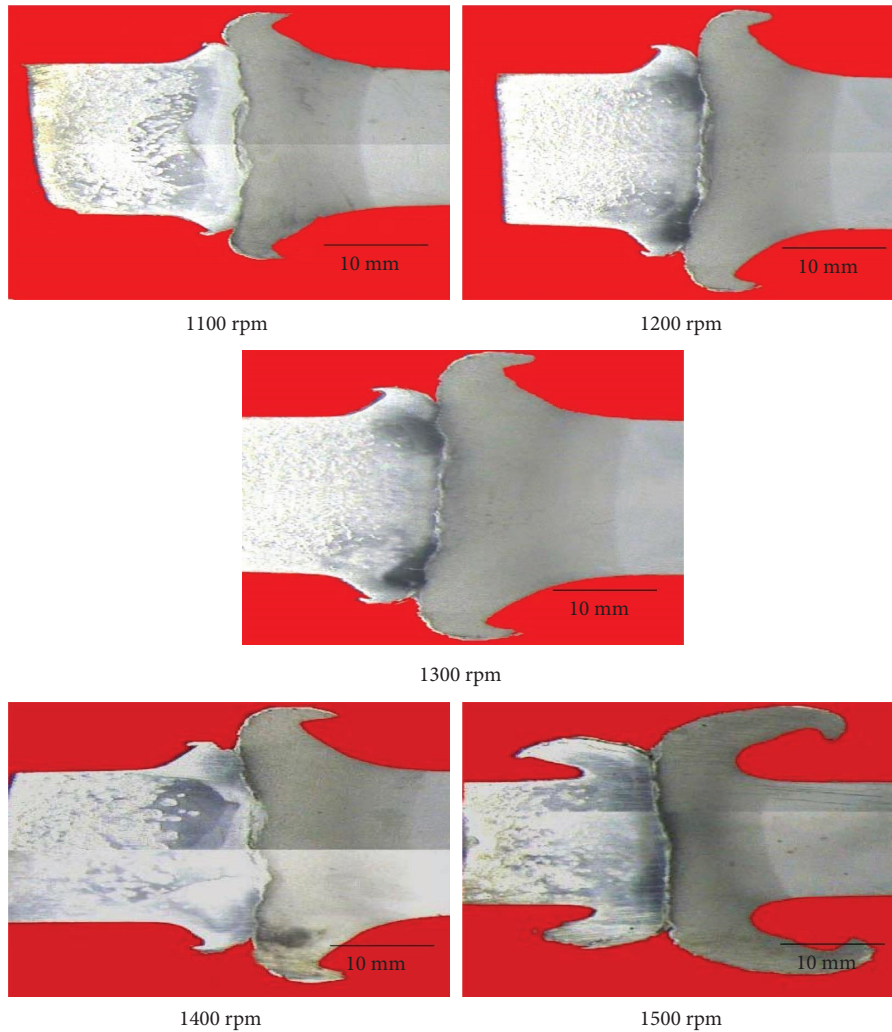


FIGURE 4: Macrostructure of dissimilar friction welded joints.

superalloy demonstrates its high-temperature strength and toughness as well as its corrosion resistance. Increased high-temperature characteristics of the nickel-based superalloy are achieved through the inclusion of cobalt, molybdenum, nickel, and other alloying components (SU 718).

**3.3. Microstructure Characterization.** All of the welding settings were used to demonstrate the microstructures at the interface area and several other locations of the rotary friction welded Inconel 718 to martensitic stainless steel AISI 410 dissimilar joints including the full deformed zone (FDZ), the partially deformed zone (PDZ), and the heat-affected zone (HAZ) in Figures 5 to 9. The interface area is subjected to both mechanical force and frictional heat as a result of the deformation of the contact region. As a result, at the microscopic level, recrystallization and mechanical interlocking take place, resulting in changes in grain size and mechanical characteristics. It is discovered that at rotating speeds of 1100 rpm, 1200 rpm, 1400 rpm, and 1500 rpm, the parent metal grains have become elongated and have recrystallized structures, which results in a decrease in strength after

1300 rpm. When looking at the interface layer, two distinct grain sizes can be seen, which indicates that the two materials have been adequately mixed in this area. These grains are extremely fine when looking at them perpendicular to the direction of the compressive force. By comparison, when the rotational speed is low, the grain structure is not tightly packed owing to a lack of an adequate quantity of frictional heat, resulting in incomplete plastic deformation as compared to the sample when the rotational speed is 1300 RPM. As a result of the grain size being much bigger than normal, the tensile strength may have decreased. When the rotating speed is increased to 1500 rpm, the friction heat and continuous forging pressure involved increase, resulting in more heating and more molten metal being drawn away from the completely deformed zone (flash), resulting in rapid cooling in this area [31]. As a consequence, the area becomes brittle, and its mechanical characteristics are degraded.

**3.4. Microhardness Characterization.** Hardness measurements were taken from the welded zone to the base material (Inconel718) and from the welded zone to the base material

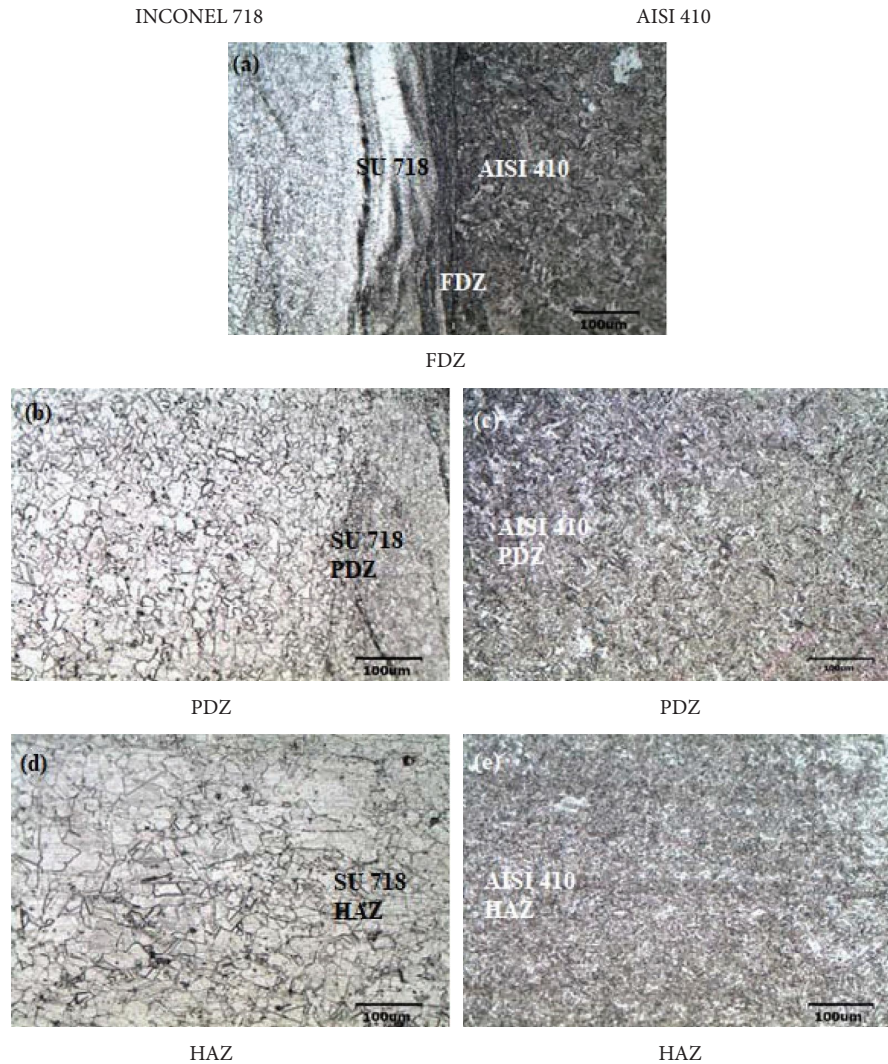


FIGURE 5: Dissimilar weld joint microstructure at 1100 rpm.

(AISI 410), and each measurement was taken from a distance of 0.1 mm from the welded zone to the base material. Figure 10 depicts a clear representation of the hardness graph. The hardness of dissimilar joints was influenced by the change in their parameters. Compared to 1100, 1200, 1400, and 1500 rpm rotational speeds, the interface hardness of the dissimilar joint of Inconel 718 and AISI 410 were higher at 1300 rpm. Meanwhile, the near PDZ of Inconel 718 hardness is higher compared to the PDZ of AISI 410 due to the high working temperature, as shown in Figure 10. In addition, the measured hardness at the HAZ on both sides was found to be lower when compared to the other region, as the region experiencing the friction heat with the absence of metal deformation action was attributed to weakening the HAZ. Despite the variation in rotation speed, the peak hardness plot was found at FDZ as the interface of the dissimilar joint experiences severe plastic deformation due to dynamic recrystallization.

**3.5. Fractography with EDS Analysis.** A scanning electron microscope (SEM) was used to analyze the fracture surfaces of the tensile-tested Inconel 718 and AISI 410 dissimilar joint

specimens to better understand the failure patterns. Figure 11 depicts a scanning electron micrograph of the fracture surface of a tensile specimen that was produced using the optimal parameters and shows the surface of the fracture. When comparing Inconel 718 and AISI 410 samples, it is possible to differentiate between the two distinct fracture surface morphologies seen in the micrograph. In Figure 11, microvoid coalescence was shown to be the most prevalent kind of fracture. This kind of fracture surface growth occurs as a result of the development of microvoids in second-phase particles during the deformation process. Dimple patterns around the graphite nodules indicate deformation of the surrounding ferrite during the last phase of training leading up to the fracture of the nodules [32–34]. It demonstrates the comparatively large cavity size as compared to the size of the graphite nodules. The hole formation may have been triggered by the graphite and its matrix losing its cohesion. The material's fracture surface was mostly comprised of brittle dimples, with a few cleavage facets scattered throughout.

As a consequence of the fracture propagating on multiple planes of varying heights, the facets are marked with river



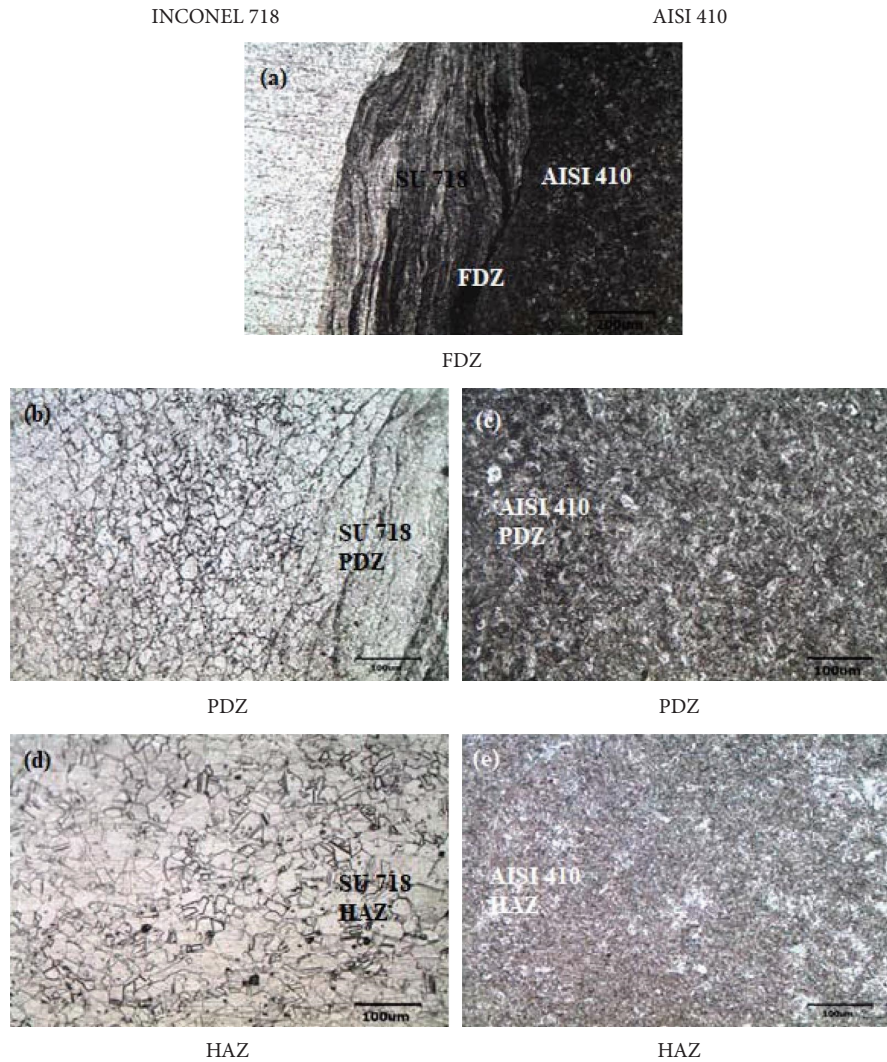


FIGURE 6: Dissimilar weld joint microstructure at 1200 rpm.

marks (see illustration). In crystallography, this kind of fracture propagates along low-index crystallographic planes has low energy [35–38] and is brittle. A microcrack developed at the graphite-matrix contact that encircled the nodule and subsequently spread to the matrix can also be observed in the micrographs. The fracture modes showed plastic deformation around the graphite nodules, and the fracture mechanisms are a combination of cleaves and dimple patterns, indicating that the heat-affected structure has been transformed into a ductile structure as a result of the welding process.

The energy-dispersive X-ray analysis (EDS) of the friction-welded Inconel 718-AISI 410 interfaces was performed using the best possible parameters throughout the portion of the interface. The findings of the EDS examination of chromium with iron distribution over the interface of Inconel 718 with AISI 410 in the axis of the dissimilar connected samples are clearly shown in Figure 12, which is visible. The records were analyzed, and it was discovered that there was a diffusion of chromium with iron, as well as a contact between Inconel 718 and AISI 410. The findings of the EDS mapping of the

distribution of chromium and iron at the interface of the Inconel 718-AISI 410 joints are shown in Figure 12. That may be seen in the maps, as well as in the AISI 410 matrix. Figure 12 shows that chromium and iron may also occur and can be dispersed in a “more uniform” manner. During friction welding, the nodular chromium and iron particles between the Inconel 718 and AISI 410 samples are deformed into ellipsoids or are even flattened, depending on the amount of force applied to the sample surface. Consequently, the chromium operates at AISI 410, which would result in greater heat generation during friction [39, 40]. Because of this, there is more heat in the friction contact zone, resulting in higher temperatures and greater diffusion coefficients in the zone. As a result, the mechanical characteristics of mechanical joints at the point of contact are substantially decreased.

The existence of this ailment was previously documented by several writers. When the microstructure was observed using various rotational speeds, it was discovered that only the chromium and iron content had been somewhat distorted and that the globular shape of the material had been maintained in

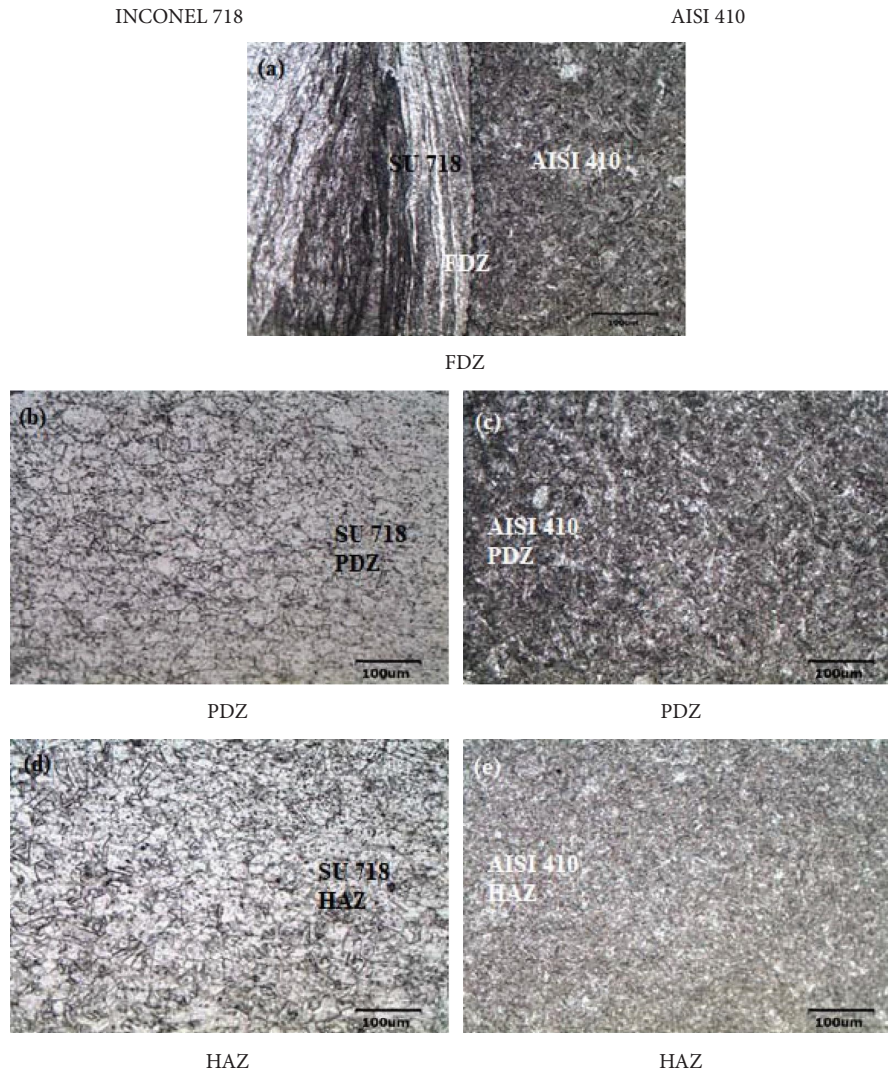


FIGURE 7: Dissimilar weld joint microstructure at 1300 rpm.

contrast to the parent material. Those findings are in agreement with the results of the EDS linear microanalysis and they corroborate the findings of hardness variations at the interface. Carbon transfer across an Inconel718-AISI410 steel interface is shown to be a consequence of friction welding, as demonstrated by the findings of this study. Steel is enriched with chromium atoms as a consequence of this process, which also results in the formation of a solid solution between steel and iron [41, 42].

**3.6. X-Ray Diffraction Analysis.** When using dissimilar friction welding, the main mechanism that enhances joint integrity is the high-temperature solid-state diffusion of different components. This occurs as a result of the simultaneous application of rotating speed and applied friction pressure in the welding process. In addition, previous study findings demonstrated that the joint strength of dissimilar joints rose with an increase in the mutual solubility of components contained in the materials that were to be connected, as previously reported. The element distribution along the friction welded Inconel 718-AISI 410 dissimilar junction was determined using an EDS line scan, which

revealed that iron is concentrated near the weld interface, while chromium and nickel varied gradually. An XRD study was performed to determine the intensity of phase presence at diffracted angles, which are presented in Figure 13. The existence of  $NbNi_3$  (38%),  $NiTi_2$  (16.2%),  $FeNi$  (16.2%),  $Fe_2Ti$  (16.2%),  $CrNiFe$  (9.8%), and  $NbC$  (3.6%) was discovered as phase compounds and the same was confirmed with alloying elements present in the base metals. The volume fraction of these compounds was calculated by taking a ratio between the particular phase intensity and the total peak intensity of all phases. Furthermore, compounds such as  $NbNi_3$ ,  $CrNiFe$ , and  $FeNi$  are identified as strengthening compounds ( $\gamma''$ ) in the nickel-based matrix. Meanwhile, the refined grain with a uniform microstructure observed in the weld interface region could be associated with the dissolution of the strengthening compound in the nickel-based matrix. In addition, iron, nickel, and chromium were all prevalent components in the intermetallic zone, as was the foundation material for Inconel 718 and AISI410, which were all developed in this region. At their highest concentrations, chromium solubility reached 0.51 percent and nickel



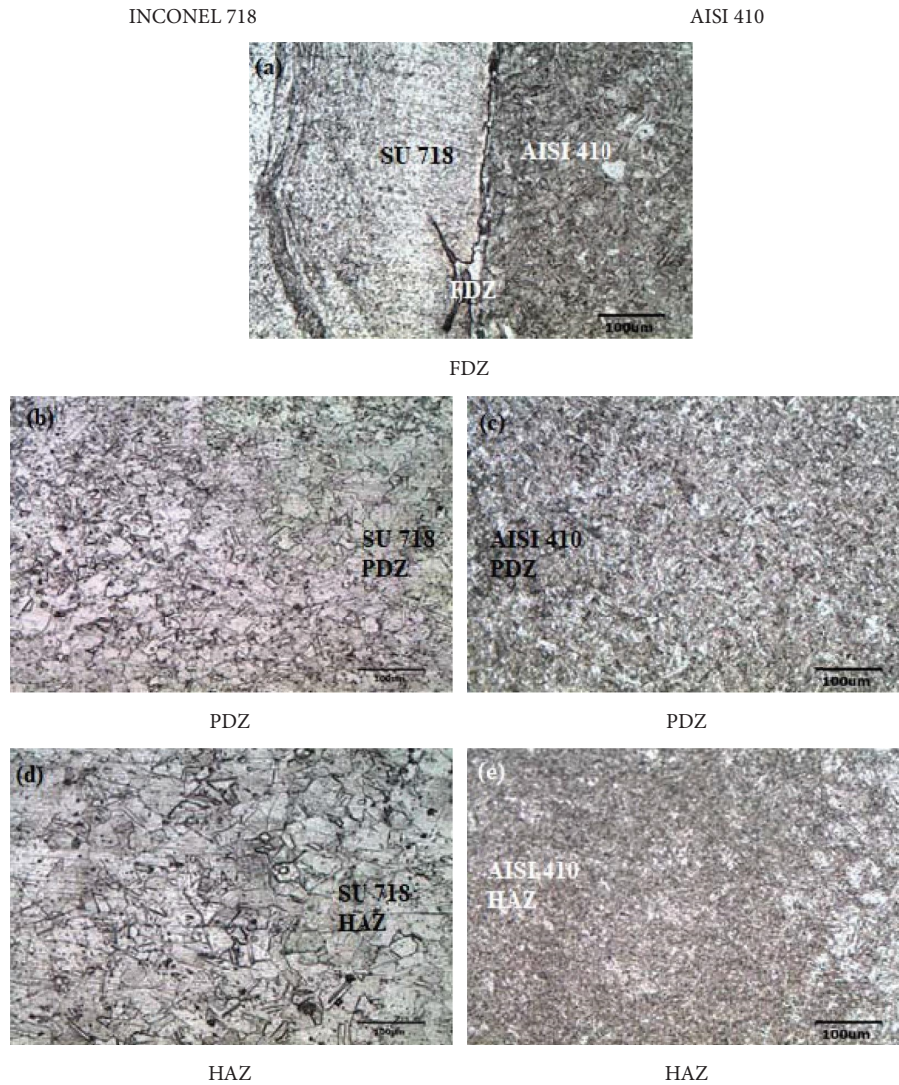


FIGURE 8: Dissimilar weld joint microstructure at 1400 rpm.

solubility reached 0.54 percent. When iron is subjected to friction, the elements chromium and nickel are readily dissolved. Iron and nickel, on the other hand, may react with the chromium present in the nickel alloy, resulting in the formation of different intermetallic compounds such as CrNiFe and FeNi. As shown in the XRD findings (Figure 13), since the mutual solubility between chromium, iron, and nickel is greater when compared to magnesium and titanium, FeNi diffused toward the steel alloy interface during friction welding, resulting in the production of CrNiFe intermetallic complex.

**3.7. Pitting Corrosion Analysis.** Figure 14 shows the polarization curve behaviour for FW dissimilar joints and parent metals. The parent metal Inconel 718 has superior corrosion potential ( $0.392 \text{ mA/cm}^2$ ) when compared to the AISI 410 MSS

parent metal, as the Inconel 718 base metal has superior mechanical properties even at high temperatures. Furthermore, the corrosion potentials for the AISI 410 MSS base metal and the dissimilar welded joint are  $0.568 \text{ mA/cm}^2$  and  $1.58 \text{ mA/cm}^2$ , respectively. The joint displayed a condensed state of corrosion current as the occurrence of dynamic recrystallization during the FW was attributed to weakening microstructure integrity, which might be the reason for this condensation. In addition, the formation of the third phase at a dissimilar interface could be the reason for increased corrosion. When compared to the optimized level, joints manufactured at speeds other than 1300 rpm have lower corrosion potentials. This is because of the occurrence of potential mode change (positive region) at 1300 rpm as the welded surface becomes partially passive with NaCl solution. The corroded samples captured by SEM shown in Figure 15 also reflect the same as the corroded region was found high in the dissimilar joint.



INCONEL 718

AISI 410

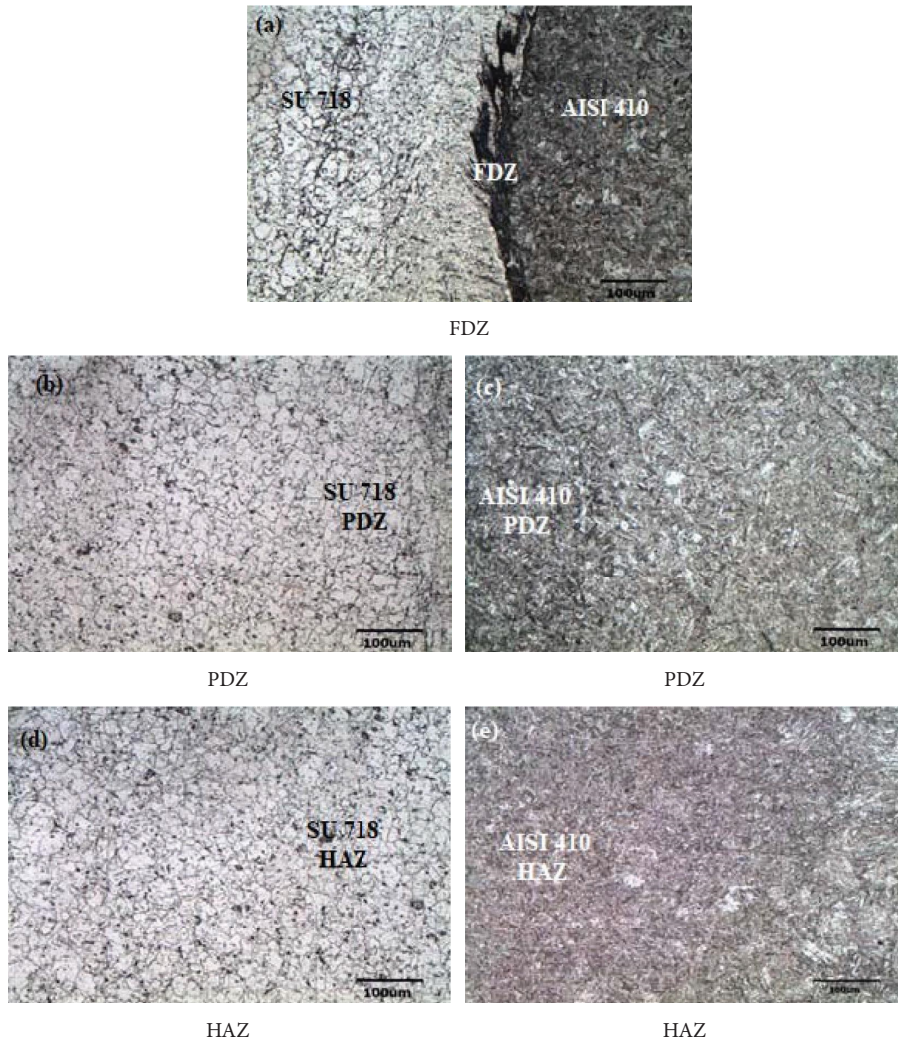


FIGURE 9: Dissimilar weld joint microstructure at 1500 rpm.

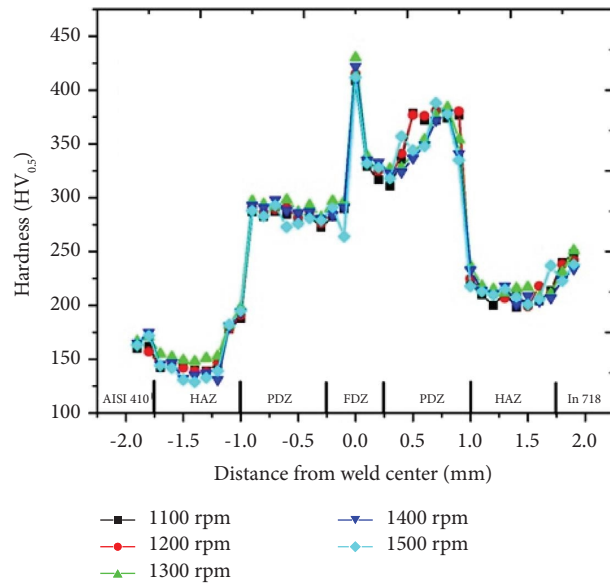


FIGURE 10: Hardness variation in different rotational speeds.

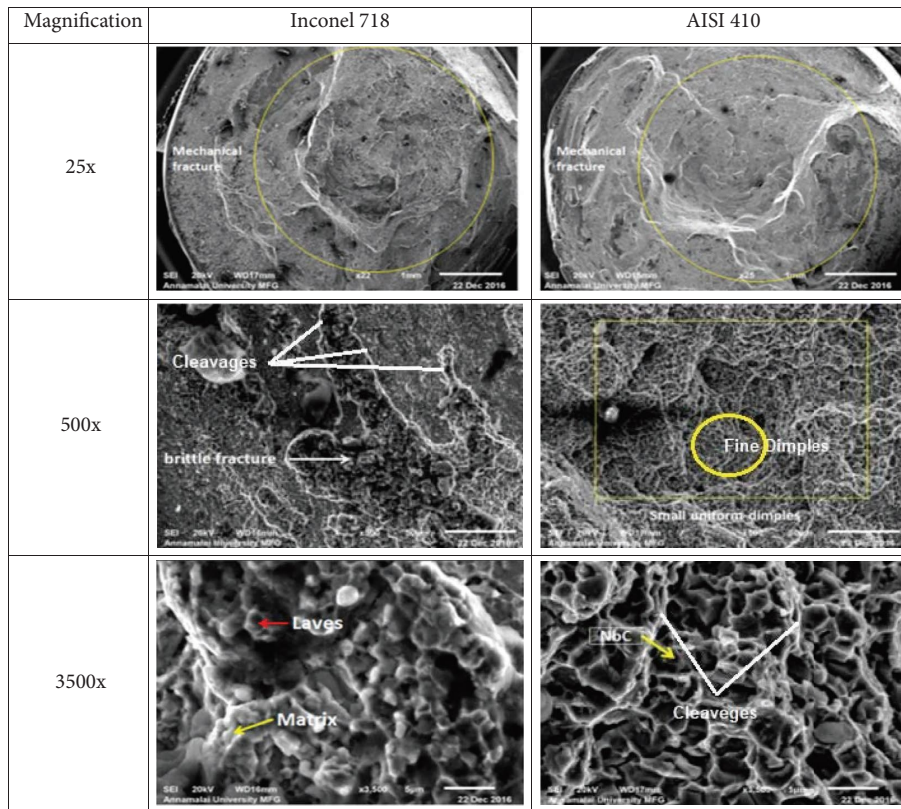


FIGURE 11: Fractography of tensile-tested samples of dissimilar friction welded joints.

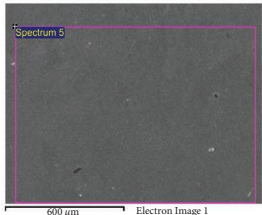
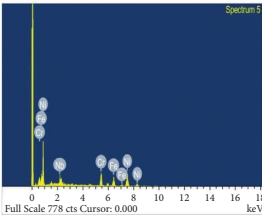
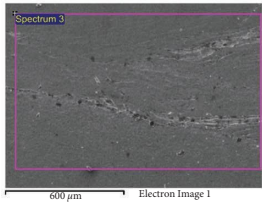
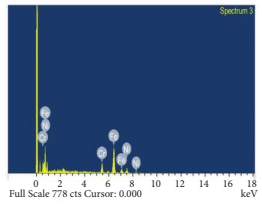
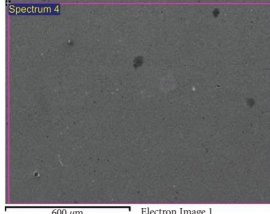
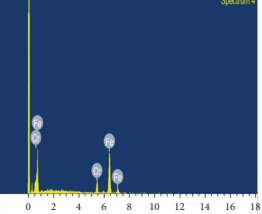
Position	Zones	Component Graph	Results																		
Fully deformed zone of Inconel 718			<table border="1"> <thead> <tr> <th>Elem...</th> <th>Weight%</th> <th>Atomic%</th> </tr> </thead> <tbody> <tr> <td>Cr K</td> <td>0.70</td> <td>22.30</td> </tr> <tr> <td>Fe K</td> <td>0.63</td> <td>18.53</td> </tr> <tr> <td>Ni K</td> <td>1.90</td> <td>53.59</td> </tr> <tr> <td>Nb L</td> <td>0.31</td> <td>5.58</td> </tr> <tr> <td>Totals</td> <td>3.54</td> <td></td> </tr> </tbody> </table>	Elem...	Weight%	Atomic%	Cr K	0.70	22.30	Fe K	0.63	18.53	Ni K	1.90	53.59	Nb L	0.31	5.58	Totals	3.54	
Elem...	Weight%	Atomic%																			
Cr K	0.70	22.30																			
Fe K	0.63	18.53																			
Ni K	1.90	53.59																			
Nb L	0.31	5.58																			
Totals	3.54																				
Fully Deformed zone			<table border="1"> <thead> <tr> <th>Elem...</th> <th>Weight%</th> <th>Atomic%</th> </tr> </thead> <tbody> <tr> <td>Cr K</td> <td>0.51</td> <td>15.81</td> </tr> <tr> <td>Fe K</td> <td>2.38</td> <td>69.35</td> </tr> <tr> <td>Ni K</td> <td>0.54</td> <td>14.84</td> </tr> <tr> <td>Totals</td> <td>3.42</td> <td></td> </tr> </tbody> </table>	Elem...	Weight%	Atomic%	Cr K	0.51	15.81	Fe K	2.38	69.35	Ni K	0.54	14.84	Totals	3.42				
Elem...	Weight%	Atomic%																			
Cr K	0.51	15.81																			
Fe K	2.38	69.35																			
Ni K	0.54	14.84																			
Totals	3.42																				
Fully Deformed zone of AISI 410			<table border="1"> <thead> <tr> <th>Elem...</th> <th>Weight%</th> <th>Atomic%</th> </tr> </thead> <tbody> <tr> <td>Cr K</td> <td>0.51</td> <td>14.09</td> </tr> <tr> <td>Fe K</td> <td>3.33</td> <td>85.91</td> </tr> <tr> <td>Totals</td> <td>3.84</td> <td></td> </tr> </tbody> </table>	Elem...	Weight%	Atomic%	Cr K	0.51	14.09	Fe K	3.33	85.91	Totals	3.84							
Elem...	Weight%	Atomic%																			
Cr K	0.51	14.09																			
Fe K	3.33	85.91																			
Totals	3.84																				

FIGURE 12: EDSSEM investigation.

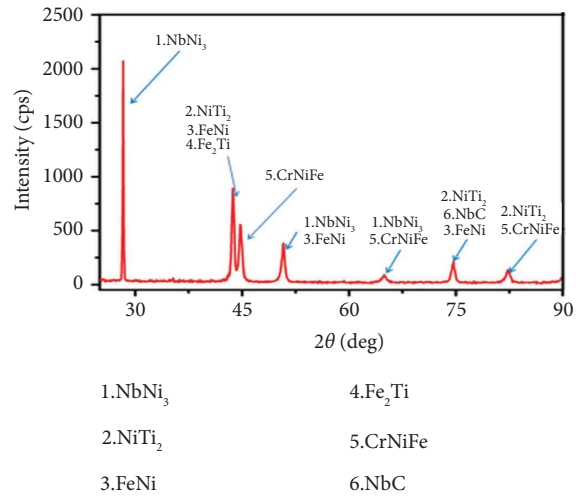


FIGURE 13: XRD pattern identified across the Inconel 718 and AISI 410 martensitic.

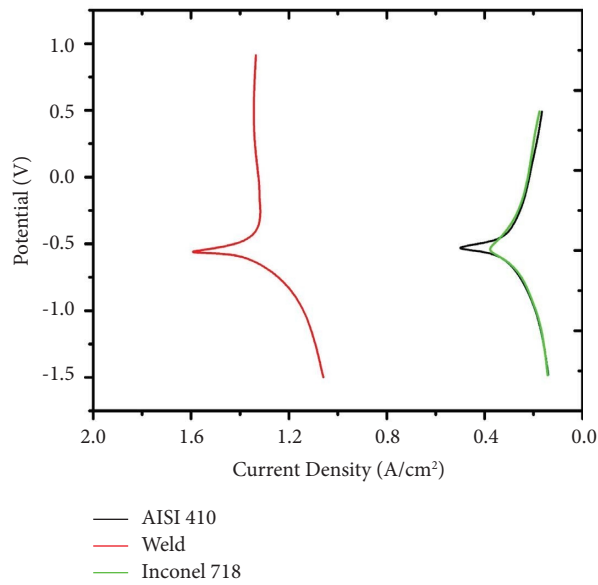


FIGURE 14: Polarization curves for base metal and weld sample.

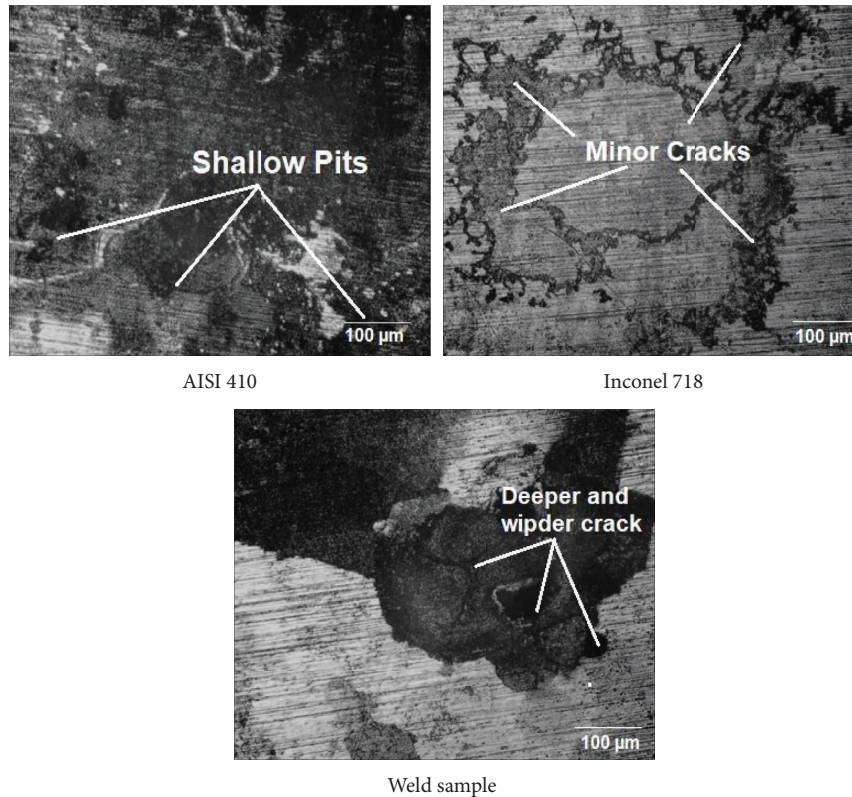


FIGURE 15: Corroded surface of base metal and weld sample.

#### 4. Conclusions

Various rotating speeds were used in conjunction with constant friction pressure, friction time, forging pressure, and forging time to achieve rotary friction welding of Inconel 718 and MSS 410 materials. The following conclusions were made from the microstructural, SEM, EDS, XRD, and mechanical property analyses, as well as from the mechanical property assessment.

- (a) One may observe high tensile strength and elongation when the rotating speed is 1300 rpm, the friction pressure is 188 MPa, the friction duration is 10 sec, the forging pressure is also 188 MPa, and the forging time is 10 sec. Tensile strength rises with increasing rotational speed up to 1300 rpm, after which it begins to decline. The failure occurs on the AISI 410 side of the test in all cases.
- (b) The highest hardness was found at FDZ, and thereafter the hardness gradually declines. When the 1300 rpm rotational speed is moved away from the interface of the five rotational speeds, it shows the greatest hardness. The findings of the hardness test are in excellent accord with those of the tensile strength test.
- (c) The hot tensile strength of steel diminishes when the temperature is raised from room temperature to 650 degrees Celsius. The lowest strength was obtained at 650 degrees Celsius, and the tensile strength of a friction-welded dissimilar joint is 44 percent lower than the tensile strength obtained at room temperature.

- (d) There are some recrystallized features in the FDZ, which results in finer grain size. At the PDZ, the grains were somewhat elongated, while at the HAZ, the granules are coarse.
- (e) EDS and XRD examination confirmed the existence of chromium concentration as well as CrNiFe intermetallics at the interface between SU-718 and AISI 410, which would result in an enhancement in the hardness and tensile strength of the dissimilar joint.

#### Data Availability

The data used to support the findings of this study are included in the article.

#### Conflicts of Interest

The authors declare that they have no conflicts of interest regarding the publication of this paper.

#### Acknowledgments

The publication is only for the academic purpose of Addis Ababa Science and Technology University, Ethiopia.

#### References

- [1] V. Ajay, N. K. Babu, M. Ashfaq, T. M. Kumar, and K. V. Krishna, "A review on rotary and linear friction welding of Inconel alloys," *Transactions of the Indian Institute of Metals*, vol. 74, no. 11, pp. 2583–2598, 2021.



- [2] R. Damodaram, S. G. S. Raman, and K. P. Rao, "Microstructure and mechanical properties of friction welded alloy 718," *Materials Science and Engineering: A*, vol. 560, pp. 781–786, 2013.
- [3] M. Bakkiyaraj, A. K. Lakshminarayanan, S. Yuvaraj, and P. K. Nagarajan, "Effect of friction time on tensile strength and metallurgical properties of friction welded dissimilar aluminum alloy joints," *Materials Testing*, vol. 63, no. 12, pp. 1097–1103, 2021.
- [4] Y. S. Kong, M. Cheepu, and D. G. Kim, "Microstructure and mechanical properties of friction-welded and post-heat-treated Inconel 718," *Transactions of the Indian Institute of Metals*, vol. 73, no. 6, pp. 1449–1453, 2020.
- [5] A. U. Rehman, Y. Usmani, A. M. Al-Samhan, and S. Anwar, "Rotary friction welding of Inconel 718 to Inconel 600," *Metals*, vol. 11, no. 2, pp. 244–253, 2021.
- [6] M. Smith, L. Bichler, J. Gholipour, and P. Wanjara, "Mechanical properties and microstructural evolution of in-service Inconel 718 superalloy repaired by linear friction welding," *International Journal of Advanced Manufacturing Technology*, vol. 90, no. 5–8, pp. 1931–1946, 2017.
- [7] S. Tabaie, F. Rézaï-Aria, B. C. D. Flipo, and M. Jahazi, "Grain size and misorientation evolution in linear friction welding of additively manufactured IN718 to forged superalloy AD730TM," *Materials Characterization*, vol. 171, Article ID 110766, 2021.
- [8] H. Wang, K. Ikeuchi, M. Aritoshi, M. Takahashi, and A. Ikeda, "Joint strength of Inconel 718 alloy and its improvement by post-weld heat treatment – joint performance and its controlling factors in friction welding of Inconel 718 alloy," *Welding International*, vol. 23, no. 9, pp. 679–686, 2009.
- [9] V. Bhanu, C. Pandey, and A. Gupta, "Dissimilar joining of the martensitic grade P91 and Incoloy 800HT alloy for AUSC boiler application: microstructure, mechanical properties and residual stresses," *CIRP Journal of Manufacturing Science and Technology*, vol. 38, pp. 560–580, 2022.
- [10] M. Anuradha, V. C. Das, D. Venkateswarlu, and M. Cheepu, "Microstructure characterization in dissimilar TIG welds of Inconel alloy 718 and high strength tensile steel," *Materials Science Forum*, vol. 969, pp. 496–501, 2019.
- [11] S. J. S. Chelladurai, K. Murugan, A. P. Ray, M. Upadhyaya, V. Narasimharaj, and S. Gnanasekaran, "Optimization of process parameters using response surface methodology: a review," *Materials Today Proceedings*, vol. 37, no. 2, pp. 1301–1304, 2021.
- [12] S. Dev, K. D. Ramkumar, N. Arivazhagan, and R. Rajendran, "Effect of continuous and pulsed current GTA welding on the performance of dissimilar welds involving aerospace grade alloys," *Transactions of the Indian Institute of Metals*, vol. 70, no. 3, pp. 729–739, 2017.
- [13] S. J. S. Chelladurai, S. Mayilswamy, A. S. Balakrishnan, and S. Gnanasekaran, *Green Materials and Advanced Manufacturing Technology: Concepts and Applications*, CRC Press, Boca Raton, FL, USA, 1st edition, 2020.
- [14] G. Dak and C. Pandey, "A critical review on dissimilar welds joint between martensitic and austenitic steel for power plant application," *Journal of Manufacturing Processes*, vol. 58, pp. 377–406, 2020.
- [15] V. T. Gaikwad, M. K. Mishra, V. D. Hiwarkar, and R. K. P. Singh, "Microstructure and mechanical properties of friction welded carbon steel (EN24) and nickel-based superalloy (IN718)," *Int. J. Miner. Metall. Mater.*, vol. 28, no. 1, pp. 111–119, 2021.
- [16] S. Gnanasekaran, G. Padmanaban, and V. Balasubramanian, "Effect of laser power on metallurgical, mechanical and tribological characteristics of hardfaced surfaces of nickel-based alloy," *Lasers Manuf. Mater. Process*, vol. 4, no. 4, pp. 178–192, 2017.
- [17] Y. Li, X. Guo, B. Chen et al., "Microstructure and mechanical properties of linear friction welding joint of GH4169 alloy/S31042 steel," *Jinshu Xuebao/Acta Metall. Sin.* vol. 57, no. 3, pp. 363–374, 2021.
- [18] G. Senthilkumar and R. Ramakrishnan, "A study of individual and interaction effect of process parameters on friction welded AISI 410 and AISI 430 joint," *Materials Today Proceedings*, vol. 46, pp. 3233–3239, 2021.
- [19] J. Alex Anandaraj, S. Rajakumar, V. Balasubramanian, and V. Petley, "Investigation on mechanical and metallurgical properties of rotary friction welded In718/SS410 dissimilar materials," *Materials Today Proceedings*, vol. 45, pp. 962–966, 2021.
- [20] P. Anitha, M. C. Majumder, V. Saravanan, and S. Rajakumar, "Effect of burn-off length for friction welded dissimilar joints of Inconel 718 and SS410," *Journal of Advances in Mechanical Engineering and Science*, vol. 4, no. 1, pp. 30–37, 2018.
- [21] A. A. Negemiya, S. Rajakumar, and V. Balasubramanian, "A study on the interface microstructure of diffusion bonded AISI410/su718 dissimilar joints," *Journal of Advanced Microscopy Research*, vol. 13, no. 1, pp. 61–64, 2018.
- [22] A. K. Maurya, C. Pandey, and R. Chhibber, "Dissimilar welding of duplex stainless steel with Ni alloys: a review," *International Journal of Pressure Vessels and Piping*, vol. 192, Article ID 104439, 2021.
- [23] M. Cheepu and W. S. Che, "Characterization of interfacial microstructure in friction welds between Inconel 718 and SM45C steel," *Transactions of the Indian Institute of Metals*, vol. 73, no. 6, pp. 1567–1571, 2020.
- [24] S. Dev, K. D. Ramkumar, N. Arivazhagan, and R. Rajendran, "Investigations on the microstructure and mechanical properties of dissimilar welds of Inconel 718 and Sulphur rich martensitic stainless steel, AISI 416," *Journal of Manufacturing Processes*, vol. 32, pp. 685–698, 2018.
- [25] M. Bakkiyaraj, G. Saikrishnan, and V. Balasubramanian, "Estimating the mechanical properties of friction welded AISI 410 MSS joints using empirical relationship," *Metall. Res. Technol.*, vol. 117, no. 6, pp. 618–8, 2020.
- [26] C. Pandey, "Mechanical and metallurgical characterization of dissimilar P92/SS304 L welded joints under varying heat treatment regimes," *Metallurgical and Materials Transactions A: Physical Metallurgy and Materials Science*, vol. 51, no. 5, pp. 2126–2142, 2020.
- [27] N. Bozzolo and M. Bernacki, "Viewpoint on the formation and evolution of annealing twins during thermomechanical processing of FCC metals and alloys," *Metallurgical and Materials Transactions A*, vol. 51, no. 6, pp. 2665–2684, 2020.
- [28] D. Sidharth, D. Sidharth, P. P. K. V. and S. Narayanan, "Microstructure and properties of Inconel 718 and AISI 416 laser welded joints," *Journal of Materials Processing Technology*, vol. 266, pp. 52–62, 2019.
- [29] Y. S. Kong, M. Cheepu, and J. K. Lee, "Evaluation of the mechanical properties of Inconel 718 to SCM 440 dissimilar friction welding through real-time monitoring of the acoustic emission system," *Proceedings of the Institution of Mechanical Engineers - Part L: Journal of Materials: Design and Applications*, vol. 235, no. 5, pp. 1181–1190, 2021.
- [30] P. Anitha, M. C. Majumder, V. Saravanan, and S. Rajakumar, "Microstructural characterization and mechanical properties



- of friction-welded IN718 and SS410 dissimilar joint,” *Metall. Microstruct. Anal.*, vol. 7, no. 3, pp. 277–287, 2018.
- [31] A. Arun Negemiya, S. Rajakumar, and V. Balasubramanian, “Influence of high temperature diffusion bonding process parameters on mechanical and metallurgical characteristics of nickel superalloy to martensitic stainless steel,” *Microscopy Research and Technique*, vol. 83, no. 3, pp. 318–328, 2020.
- [32] S. V. Lalam, G. M. Reddy, T. Mohandas, M. Kamaraj, and B. S. Murty, “Continuous drive friction welding of Inconel 718 and EN24 dissimilar metal combination,” *Materials Science and Technology*, vol. 25, no. 7, pp. 851–861, 2009.
- [33] J. Senthilkumar, M. Bakkiyaraj, M. Balasubramanian, and T. G. Loganathan, “Effect of FW conditions on mechanical and microstructural characteristic of AA6061/SiC/Graphite hybrid composites joint by empirical relationship,” *Surface Topography: Metrology and Properties*, vol. 9, no. 4, 2021.
- [34] S. A. Etesami, M. H. Enayati, F. Karimzadeh, and V. Rasta, “Investigating the properties of friction welded 2014 aluminum joints prepared with different rotational speeds,” *Transactions of the Indian Institute of Metals*, vol. 68, no. 3, pp. 479–489, 2015.
- [35] M. Bakkiyaraj, P. Palanisamy, and V. Balasubramanian, “Evaluating the tensile strength of friction welded (AA6061 & AA7075-T6) dissimilar joints by using response surface methodology,” *Materials Research Express*, vol. 6, no. 8, Article ID 086527, 2019.
- [36] C. Pandey, N. Saini, M. M. Mahapatra, and P. Kumar, “Study of the fracture surface morphology of impact and tensile tested cast and forged (C&F) Grade 91 steel at room temperature for different heat treatment regimes,” *Engineering Failure Analysis*, vol. 71, pp. 131–147, 2017.
- [37] M. Kimura, K. Suzuki, M. Kusaka, and K. Kaizu, “Effect of friction welding condition on joining phenomena and mechanical properties of friction welded joint between 6063 aluminium alloy and AISI 304 stainless steel,” *Journal of Manufacturing Processes*, vol. 26, pp. 178–187, 2017.
- [38] R. M. Landell, C. R. De Lima Lessa, L. Bergmann, J. F. Dos Santos, C. E. F. Kwietniewski, and B. Klusemann, “Investigation of friction stir welding process applied to ASTM 572 steel plate clad with Inconel 625,” *Welding in the World*, vol. 65, no. 3, pp. 393–403, 2020.
- [39] R. Moradi, M. Roshanaee, H. Mostaan, F. Nematzadeh, and M. Safari, “Microstructural studies on laser welding of Inconel 718 to 2304 duplex stainless steel with a focus on optimizing process parameters and achieving the maximum fracture strength,” *J. Adv. Mater. Eng.*, vol. 40, no. 1, pp. 45–63, 2021.
- [40] S. Kumar, S. Kumar, C. Pandey, and A. Goyala, “Effect of post-weld heat treatment and dissimilar filler metal composition on the microstructural developments, and mechanical properties of gas tungsten arc welded joint of P91 steel,” *International Journal of Pressure Vessels and Piping*, vol. 191, 2021.
- [41] P. Sathiya, S. Aravindan, and A. Noorul Haq, “Effect of friction welding parameters on mechanical and metallurgical properties of ferritic stainless steel,” *International Journal of Advanced Manufacturing Technology*, vol. 31, no. 11-12, pp. 1076–1082, 2007.
- [42] N. Ozdemir, “Investigation of the mechanical properties of friction-welded joints between AISI 304L and AISI 4340 steel as a function rotational speed,” *Materials Letters*, vol. 59, no. 19-20, pp. 2504–2509, 2005.